Incorporating Vegetation in Solar Chimney Power Plant: A Northern Algerian Site Study

Semai, Hakim
Renewable Energy Development Center (CDER), Solar Thermal and Geothermal Energy Division

Bouhdjar, Amor
Renewable Energy Development Center (CDER), Solar Thermal and Geothermal Energy Division

https://doi.org/10.5109/7183365

出版情報：Evergreen. 11 (2), pp.846-861, 2024-06. 九州大学グリーンテクノロジー研究教育センター
バージョン：

Incorporating Vegetation in Solar Chimney Power Plant: A Northern Algerian Site Study

Hakim Semai[1,*] Amor Bouhdjar[1]
[1]Renewable Energy Development Center (CDER), Solar Thermal and Geothermal Energy Division, 16340 Bouzaréah Algiers, Algeria

*Author to whom correspondence should be addressed:
E-mail : hsemai@yahoo.com, h.semai@cder.dz

(Received February 27, 2024; Revised May 15, 2024; Accepted June 2, 2024).

Abstract: This study presents a numerical simulation of a solar chimney power plant with and without vegetation, aiming to investigate the impact of incorporating plant cultivation at the collector level. The simulation, conducted for two typical days (30-12-2021 and 04-01-2022), explores the variations in fluid temperature and velocity inside the collector in response to solar radiation and the ambient temperature specific to the Bouzaréah site in northern Algeria. The presence of vegetation, represented by tomato cultivation, demonstrates significant effects on system performance. The collector's efficiency exhibits notable differences between scenarios with and without vegetation, with the vegetation-free system-performing better during periods of intense sunlight. However, as solar radiation diminishes towards the end of the day, the system with vegetation outperforms, highlighting its resilience in lower radiation conditions. The internal conditions of the collector, especially in the presence of vegetation, appear conducive to plant growth. Interestingly, the study concludes that the presence of vegetation does not adversely affect the overall efficiency of the solar chimney power plant. On the contrary, integrating vegetation at the collector level enhances the overall efficiency of the solar chimney power plant, potentially reducing the cost per kilowatt-hour produced and, consequently, shortening the payback period for the initial investment. This study provides valuable insights for further exploration of this hybrid approach in the field of solar energy.

Keywords: solar chimney, vegetation, efficiency, energy, heat, turbulent

1. Introduction

The shift towards renewable energy sources has become imperative in our rapidly changing world to preserve our environment and ensure a sustainable future for humanity[1, 2]. This transition is motivated by several critical factors. The use of traditional fossil fuels like coal, oil, and natural gas has led to severe environmental consequences, including air and water pollution, deforestation, and greenhouse gas emissions[3-5]. These emissions are major contributors to climate change, which poses unprecedented risks to our planet's ecosystems, weather patterns, and sea levels. Renewable energy sources such as solar, wind, hydroelectric, and geothermal power offer clean and sustainable alternatives. Unlike fossil fuels, renewable energy technologies produce little to no greenhouse gas emissions during operation, thereby mitigating climate change impacts. Furthermore, renewable energy is abundant and widely distributed, offering a decentralized energy system that can enhance energy security and resilience. Transitioning to renewable energy is also crucial for ensuring energy access and affordability for all. As technology advances and economies of scale drive down costs, renewable energy has become increasingly cost-competitive with fossil fuels. Investing in renewables not only reduces our reliance on finite and polluting energy sources but also creates new economic opportunities, including job growth in the green energy sector. Innovative approaches such as solar chimney power plants highlight the potential of renewable energy to address multiple needs simultaneously. Solar chimneys harness solar radiation to create an updraft within a tall chimney, driving turbines to generate electricity[6]. This technology not only taps into clean energy but also offers scalability and adaptability in various regions.

Solar chimney stands out as an ingenious low-temperature system within the realm of renewable energy. Its simplicity in design, utilization of locally sourced materials, and minimal labor requirements

distinguish it from other renewable energy technologies.

In addition, integrating renewable energy infrastructure like solar collector in solar chimney power plant with dual-purpose applications, such as using the collector structures for agricultural greenhouses, presents an opportunity to reduce the kilowatt-hour cost and enhance resource efficiency. By maximizing land and infrastructure use through dual-functionality, we can optimize energy production while supporting local agriculture and food security.

Its extensive surface area optimizes the absorption of solar energy, heating the air essential for turbine rotation while simultaneously creating an environment conducive to agricultural cultivation. The integration of energy production ~~with~~ and agricultural space means a unique synergy, leveraging the solar chimney's capabilities to foster a sustainable ecosystem where electricity generation and crop cultivation coexist harmoniously, emphasizing the multifaceted advantages of this innovative approach.

The widespread interest in renewable energies is highlighted through numerous theoretical and experimental studies conducted by many researchers. Specifically concerning low-temperature systems like solar chimney power plants, most of these studies have cited the experimental prototype of Manzanares carried out in Spain [7, 8].

Research and experimentation in the field of solar chimneys have demonstrated their viability as a reliable energy source. The Manzanares prototype in Spain, operational from 1982 to 1989[9], serves as tangible evidence of the technology's reliability and potential for successful energy transition. Many studies have focused on enhancing the system's efficiency through various geometric configurations and operational parameters.

Subsequent studies have followed to delve deeper into enhancing the efficiency of this system[10-14], a crucial performance indicator. Some works are experimental[15-17], while others are theoretical[18-20].

Some of these studies have tackled the geometric aspect of the power plant, examining various configurations to assess the influence of geometric characteristics such as the height and diameter of the chimney and its geometric shape [19, 21-23], as well as the collector surface extent and its shape [19, 22, 24]. Other studies have focused on the operational aspect, examining flow parameters [25] and the physical characteristics of the transparent material, along with other key components of the power plant [26]. Additionally, research has been conducted on the wind turbines used to convert the fluid kinetic energy into electrical energy[19, 27, 28]. However, considering the significance and number of studies conducted, along with the results obtained, it can be said that the technology of solar chimney power plants has reached a considerable level of technological maturity. Despite this technological maturity achieved by solar chimney power plants, a major drawback of renewable energy systems remains their high implementation cost[29-31]. Various studies have explored alternative approaches to mitigate these costs, including the use of affordable materials for construction and optimization of collector design for dual-purpose applications like greenhouse farming.

Numerous studies have explored several alternatives to alleviate the initial cost, including:

- Considering a floating chimney tower constructed from materials with affordable prices[32-34].
- Using a mountainside as support for the tower [35, 36].
- Replacing the collector cover currently made of glass, with plastic[37-39].
- Optimizing the initial investment by considering cultivation within the solar chimney power plant collector.

Greenhouse farming is a well-developed and mastered technique owing to various research endeavors[40-47]. Research conducted in this field has significantly enhanced the productivity, sustainability, and profitability of greenhouse farming, paving the way for more efficient and environmentally friendly agricultural practices. Among the main developed areas, we can mention:

1. Environmental optimization[40, 48, 49]: Studies have been conducted to monitor and enhance the environmental conditions within greenhouses, including temperature, humidity, light, and ventilation. This involves using sensors, automated control systems, and new technologies to create optimal growth conditions.
2. Plant irrigation and nutrition [40, 45, 50, 51]: Research has been conducted to enhance irrigation and fertilization systems, employing techniques like drip irrigation, hydroponics, and fertigation to precisely provide water and nutrients to plants.
3. Disease and pest control [45, 52]: Biological control methods, including the use of beneficial organisms and integrated pest management techniques, have been developed to reduce pesticide usage and preserve crop health.
4. Plant variety selection and improvement [53, 54]: Research has been conducted to develop plant varieties specifically tailored for greenhouse cultivation, exhibiting characteristics such as disease resistance, tolerance to controlled environmental conditions, and improved yield.
5. Sustainability and energy efficiency [55]: Efforts have also focused on reducing energy consumption, utilizing renewable energy sources,

and developing sustainable greenhouses to minimize the environmental footprint of this cultivation method.

In the present work, we will simulate fluid flow in a solar chimney power plant while considering cultivation of tomatoes within the collector. This approach will allow us to observe the interaction between crop and solar chimney power plant performance.

2. Physical model

Two Solar Chimney Power Plant (SCPP) configurations are considered, both sharing the same dimensions. The chimney stands at 200 meters in height and 10 meters in diameter. The collector has a diameter of 244 meters and its cover is 3 meters above the ground level. A section of the ground, 5 meters deep, has been considered to assess its storage effect. Figure 1a shows the configuration without cultivation, while Figure. 1b displays the second configuration with tomato cultivation. In this case, vegetation is arranged in rows of length L, width l, and average height h. Two sets are formed, each consisting of n rows of tomatoes. The layout occupies half of the collector surface. Each set alternates with an empty space, meaning no planting. Rows start 2 meters away from the collector entrance and extend ~~to~~ 15 meters far from the collector exit. The predicted height of the vegetation is 2 meters, leaving 1 meter space between the-vegetation and the transparent cover. SCPP dimensions are given, according to the considered configuration, on Table 1.

Table 1. Configurations for SCPP considered for the study.

	SCPP with crop	SCPP without crop
Chimney diameter (m)	10	10
Chimney height (m)	200	200
Collector diameter (m)	244	244
Collector height (m)	3	3
Soil depth (m)	5	5
Plant height (m)	2	-
Plant width (m)	1	-
Distance between the collector inlet and the plant (m)	2	-
Distance between the plant and the collector outlet (m)	15	-
Distance between the upper surface of the plant and the transparent cover (m)	1	-

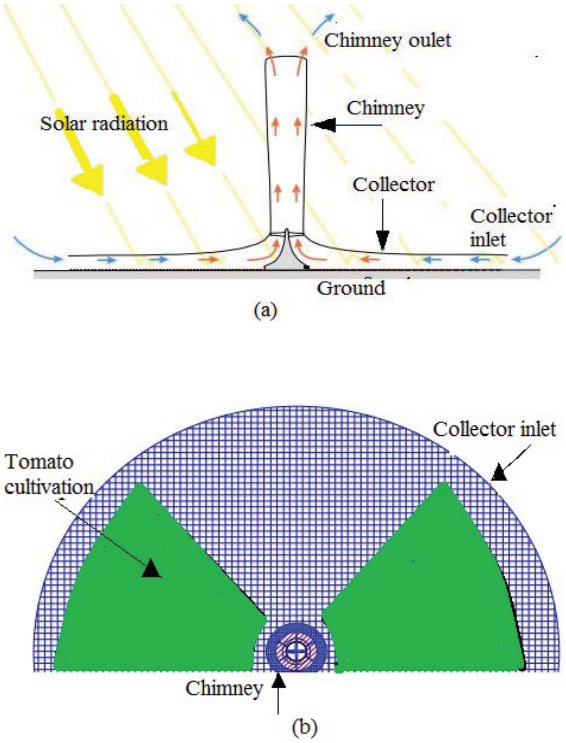

Fig. 1 : Geometry model of the SCPP; a) without crops, b) with crops.

3. Mathematical model:

3.1 SCPP without crop cultivation

In solar chimney power plant without vegetation, solving a convection problem means determining, at every point in the domain of interest and at any given time, the properties of the fluid and the fluid flow characteristics namely density (ρ), velocity components (V), temperature (T) and pressure (P). To compute these six parameters, six equations need to be generated. These equations are derived using principles of conservation of mechanics and thermodynamics. Thus, the conservation equations for mass, momentum (a vectorial equation comprising three scalar equations), and energy are obtained. Adding to that, fluid state equation is used. Gases under consideration (air, water vapor, and carbon dioxide) are assumed behaving as ideal gas. An ideal gas follows an equation of state in the form:

$$P = \rho\, r\, T \tag{1}$$

Some simplifications are assumed:

- The fluid is Newtonian (the relationship between stress and strain is linear and isotropic),
- The dynamic viscosity μ can be considered constant, neglecting bulk viscosity,
- The fluid is incompressible (its density varies slightly with pressure or temperature),
- Body forces are only due to gravitational acceleration,

- Velocities are low; hence, we neglect viscous dissipation of heat compared to diffusive heat exchange,
- Thermo-physical properties of the fluid are assumed constant,
- The fluid is completely transparent,

we present the equations governing the phenomenon of turbulent natural convection inside the collector, focusing on the balance equations governing the average fluid motion and the implications of turbulence on solving these equations. Derived governing system equations are solved using finite volume method. However, in situations, the incompressible fluid assumption is not valid, and the very slight variations in density produced by a temperature or pressure gradient must be taken into account. In the case of natural convection, flows in solar systems result from density variations due to temperature gradients within the fluid and Boussinesq approximation is assumed. It is assumed that the velocities are sufficiently low for variations in density produced by pressure changes to be negligible. This assumption holds for nearly all liquids (such as water) and for gases where $\frac{1}{2}M^2 \ll 1$ (M being the Mach number). Thus, as long as the air velocity does not exceed 100 m/s, the density can be considered independent of pressure [56]. Consequently, there is a coupling between the energy equation and the momentum equation.

In the context of natural convection, the Rayleigh number, as defined, quantifies the intensity of the flow induced by buoyancy forces.

$$R_a = \frac{g\beta(T_h - T_c){D_h}^3}{\alpha\vartheta} \quad (2)$$

The maximum and minimum temperatures in the system are denoted as T_h and T_c, respectively. D_h represents the hydraulic diameter while α stands for the thermal diffusivity. Boussinesq's approximation is used to address variations in air density. Upon analysis, it appeared that Ra>10 in both the collector and chimney, indicating a turbulent flow in these spaces[57] . The fundamental equations (mass, momentum, and energy), along with the k-ε model utilized for turbulent flows, are as follows:

$$\frac{\partial \rho}{\partial t} + \frac{\partial (u_i)}{\partial x_i} = 0 \quad (3)$$

$$\frac{\partial \mathrm{u_i}}{\partial \mathrm{t}} + \mathrm{u_j}\frac{\partial \mathrm{u_i}}{\partial \mathrm{x_j}} = -\frac{1}{\rho}.\frac{\partial \mathrm{P}}{\partial \mathrm{x_i}} + \vartheta\left(\frac{\partial^2 \mathrm{u_i}}{\partial \mathrm{x_j}\,\partial \mathrm{x_j}}\right) + \rho \mathrm{f_i} \quad (4)$$

$$\frac{\partial}{\partial \mathrm{t}}\left(\rho \mathrm{c_p T}\right) + \frac{\partial}{\partial \mathrm{x_j}}\left(\rho \mathrm{u_j c_p T}\right) = \frac{\partial}{\partial \mathrm{x_j}}\left(\lambda \frac{\partial \mathrm{T}}{\partial \mathrm{x_j}}\right) + \mathrm{T}\beta\frac{\partial \mathrm{P}}{\partial \mathrm{t}} + \emptyset \quad (5)$$

$$\frac{\partial}{\partial t}(\rho k) + \frac{\partial}{\partial x_i}(\rho k u_i) = \frac{\partial}{\partial x_j}\left(\left(\mu + \frac{\mu_t}{\sigma_K}\right)\frac{\partial k}{\partial x_j}\right) + G_K + G_b - \rho\varepsilon + S_K \quad (6)$$

$$\frac{\partial}{\partial t}(\rho\varepsilon) + \frac{\partial}{\partial x_i}(\rho\varepsilon u_i) = \frac{\partial}{\partial x_j}\left(\left(\mu + \frac{\mu_t}{\sigma_\varepsilon}\right)\frac{\partial \varepsilon}{\partial x_j}\right) + C_{1\varepsilon}(G_K + C_{3\varepsilon}G_b) - C_{2\varepsilon}\rho\frac{\varepsilon^2}{K} + S_\varepsilon \quad (7)$$

G_k stands for turbulence kinetic energy generation attributed to the mean velocity gradients: $G_k = -\rho\overline{u_i' u_j'}\frac{\partial u_j}{\partial x_i}$; G_b signifies turbulence generation due to buoyancy; σ_k *and* $\sigma_\varepsilon$denote the turbulent Prandtl numbers for k *and* ε, respectively; and β represents the thermal expansion coefficient, approximated for an ideal gas by $\beta \approx {}^{1}/_{T}$.

3.2 SCPP with vegetation

In the field of greenhouses, most available studies address the issues of cooling, heating, and ventilation. Modeling these aspects is complex due to the interaction of several surfaces, particularly with vegetation, making it even more challenging as this modeling involves other disciplines like agronomy.

Previously, we presented the equations governing the flow of a homogeneous fluid (without the presence of vegetation); now, we will discuss the case of a fluid that can be a mixture of several species. In the case of an SCPP with vegetation, the fluid is a mixture of air and water vapor. The equation concerning water vapor in the framework of irreversible thermodynamics is given as follows (Fick's law):

$$\frac{\partial w}{\partial t} + \vec{\nabla}.(w\overrightarrow{V}) - \vec{\nabla}.\vec{j} = S_{w,p} \quad (8)$$

$$\vec{j} = -D_w(\vec{\nabla}\, w + \frac{a}{T}\vec{\nabla}T) \quad (9)$$

For water vapor, we will use the Schirmer relation, applicable between 20°C and 90°C, to evaluate D_w:

$$D_w = 2{,}26\,.\,10^{-5}\frac{1}{P}\left(\frac{T}{273}\right)^{1.81} \quad (10)$$

With T in Kelvin and P in bar (for T=297K and P=1bar, D_w= 2, 26. $10^{-5}m^2.s^{-1}$).
If the mixture is very dilute, we can, as a first approximation, take Dw as constant. Thus, the movement of water vapor, considered as an incompressible fluid, is described as follows:

$$\frac{\partial w}{\partial t} + \vec{\nabla}.\left(w\,\vec{V}\right) = D_w\vec{\nabla}^2 w + S_{w,p} \quad (11)$$

This equation is strictly identical to the heat equation for an incompressible fluid when neglecting all volumetric sources.

Finally, we will need to determine six variables (u, v, w, P, T, and w) using the system of six equations that forms the closed system as presented earlier [eq. 3-7], along with the mass transfer equation (eq. 11).

4. Boundary Conditions

The boundary conditions such as solar irradiance and ambient temperature considered for the two days (30-12-2021 and 04-01-2022) are defined based on the meteorological data recorded at the Bouzaréah site (north region of Algeria).

The measurements of global solar radiation used in our study come from a pyranometer installed at a test bench comprising a solar collector field (solar water heater - air collector). These measurements, obtained on a 36° inclined plane, will be used as boundary conditions due to the lack of measurements on a horizontal plane.

4.1 SCPP without vegetation

In this case, boundary conditions include solar radiation as the sole energy source and ambient temperature as the system's inlet temperature (collector). At the collector level, the relative static pressure at the inlet is zero.

$$P_{r,inlet} = 0, T_{inlet} = T_{\infty} \quad (12)$$

Regarding the chimney wall, the boundary conditions are specified as follows:

$$\frac{\partial T}{\partial x} = 0, \quad u = 0,\ v = 0 \quad (13)$$

The temperature remains constant at a depth of 5 meters in the ground ~~soil~~, set at 300K. The heat transfer coefficient of the ground is defined by:

$$U_b = \frac{2b}{\sqrt{\pi t}} \quad (14)$$

Where t is represents the elapsed time since midnight. The thermal penetration coefficient is expressed by:

$$b = \sqrt{\lambda\, \rho\, c_p} \quad (15)$$

The collector is characterized by a transparent cover and an absorbent soil through the product of the soil absorptivity and the cover transmissivity τα=0.64

4.2 SCPP with vegetation

The climatic conditions near the ground arise from heat and mass exchanges between the soil, vegetation, and the atmosphere. Therefore, the greenhouse agro-system can be described through energy and mass transfers. These transfers occur in three forms: radiation, convection, and conduction. The mathematical modeling reflecting these phenomena leads to solving a system of equations, defined previously (eq. 3-7, 11), using numerical or analytical methods.

Due to the complex geometry of the vegetation cover, the plants are likened to a porous medium. It is assumed that the solid matrix remains rigid (or undergoes negligible deformation). In vegetation, the size and distribution of pores, equated to voids between leaves and branches, are irregular. The porosity Φ of a porous medium is defined as the ratio of the volume of the voids to the total volume occupied by the whole medium. Consequently, the solid fraction is equal to 1−Φ.

Assuming vegetation cover ~~to~~ as a porous medium is one of the few available approaches that allow the influence of plant cover on the flow to be taken into consideration.

A detailed description seems unrealistic and cannot be conducted within the scope of this study.

In addition to their influence on flow dynamics, plants also significantly alter the overall energy balance. If the crop is considered a porous medium in terms of flow resistance, it must also be considered as a source or as sink of latent and sensible heat. The net radiation at the vegetation cover scale is balanced by major components: latent heat, sensible heat, heat flux in the soil, and minor components such as photosynthesis, evapotranspiration, and stored heat. The contribution of photosynthesis and evapotranspiration to the energy balance above the cover is negligible, representing only a few percent of the net radiation [58].

The porous medium approach and the constraints arising from the detailed description of the cover's geometry lead us to adopt a macroscopic approach to describe the cover effects. Thus, we need to perform an energy balance on a volume element. In our case, the vegetation is arranged in n rows with a length L, width l, and an average height h. The area occupied by the vegetation is defined as S_cultivated=n.L.l. It is necessary to define a Volumetric Leaf Area Index (LAIv) relative to a volume of vegetation to calculate the attenuation of the incident radiation.

$$LAI_v = \frac{S_{leaf}}{S_{cultivated}.h} = \frac{S_{ground}LAI_s}{S_{cultivated}.h} \quad (16)$$

Where $LAI_s = \frac{S_{leaf}}{S_{ground}}$ (specific leaf area index)

The attenuation of the incident radiation as it penetrates the cover follows Beer's law:

$$R(z) = R_n.\exp\left(-K_c.LAI_s.\frac{z}{h}\right) \quad (17)$$

With:

R_n: Net radiation received at the cover level (w/m^2),

K_c: Radiation extinction coefficient,

h: Height of the crop,

z: Height of the level considered.

Thus, a volume element ($d\tau = dS.dz$) receives a radiative flux (eq. 18) and loses heat through evaporation, convection, and conduction with the nearby environment.

$$G(z) = \frac{dR(z)}{dz} \quad (18)$$

The balance on volume element $d\tau$ becomes:

$$\frac{dR(z)}{dz} - L_V E.LAI_V - C.2LAI_V = 0 \quad (19)$$

Where:

$R(z)$: Density of incident radiative flux per unit surface intercepting the net radiation (w/m²),

$L_V E$: Density of latent heat flux, L_V being the heat of vaporization of water (LV=2440.10^3 KJ.kg^{-1} at 20°C), and E the evaporation flux (kg.m^{-2}.s^{-1}),

C: Density of sensible heat flux (w/m²).

Leaves receive a net radiation Rn from solar radiation during the day; they release latent heat L_vE through the evaporation of the water they contain. Tomato leaves primarily exchange water vapor on the underside [59]. They also exchange sensible heat C on each side of their surface with the surrounding fluid. The L_vE and C fluxes can be expressed generally as follows:

$$C = \rho C_p \frac{T_s - T_a}{r_a} \quad (20)$$

Where ρ is the air density (kg/m³), C_p is the specific heat at constant pressure (J/kg.K),

Ts represents the temperature of the considered surface and Ta stands for the ambient air temperature. The aerodynamic resistance to heat transfer is $ra\ (s/m)$ and is calculated as:

$$r_a = \frac{\rho C_p}{h_a} = 893\left(\frac{L}{\Delta T}\right)^{0.25} \quad (21)$$

$$\Delta T = \left|T_f - T_a\right| \quad (22)$$

The water vapor flux is calculated at the vegetation level using the equation:

$$E = \rho.\frac{w_f - w_a}{r_t} \quad (23)$$

Where w_f represents the absolute saturation humidity of the considered vegetation cover layer, and w_a is the absolute humidity of the air. r_t is the total resistance to water vapor transfer for a given layer. For a tomato crop, this corresponds to the series association of aerodynamic resistance (ra) and stoma resistances (rs) of the upper and lower sides of leaves from the considered level.

From an eco-physiological perspective, the value of leaf stoma resistance depends on soil water potential, incident solar radiation [60], air saturation deficit [61], and leaf temperature [62]. In greenhouse cultivation, the soil water potential has a negligible impact on stoma close to zero due to the irrigation system. Under these optimal conditions, the baseline stoma resistance for tomatoes is around 150 s/m [59]. However, this represents a minimum value, as it is observed to evolve based on radiation, temperature, and saturation deficit.

For greenhouse tomato conditions, the function describing the evolution of rs based on the saturation deficit D is given as:

$$r_s = r_{s,min}[1 + 0.44.\exp(0.34.(D - D_{max}))] \quad (24)$$

Where $r_{s,min} = 150\ s/m$ et $D_{max} = 10\ mbar$

Saturation deficit depends on both temperature and relative humidity, and we can relate the evolution of stoma resistance to air temperature and humidity through the following relationship:

$$r_s = r_{s,min}\left\{1 + 0.11.exp\left[0.34.\left(6{,}107.10^{\frac{7.5T}{237.5+T}} - 1629.w - D_{max}\right)\right]\right\} \quad (25)$$

To describe the source term of the conservation equation considered, we use $S_\emptyset$:

$$S_\emptyset = cphi(vphi - \emptyset) \quad (26)$$

We can then identify the $cphi$ and $vphi$ terms in this relationship with the terms appearing in the expressions for sensible heat flux (20) and latent heat flux (23):

- For temperature: $\begin{cases} cphi = \frac{\rho C_p}{r_a} \\ vphi = T_f \end{cases}$ (27)

- For humidity: $\begin{cases} cphi = \frac{\rho}{r_t} \\ vphi = w_f \end{cases}$ (28)

Where T_f and w_f are respectively the internal saturated temperature and absolute humidity of the leaves.

For the meteorological data, Figure 2 shows the variation of solar radiation and ambient temperature for two days. Figure 2-a represents the meteorological conditions recorded during December 30, 2021, and Figure 2-b represents those recorded during January 4, 2022. The recorded solar

radiation, from 9 AM to 5 PM, for these two days evolves uniformly with maximum values around 930 W/m for the December day and 960 W/m for the January day. For the minimum, they are around 200 W/m for both days. Similarly, the temperature evolves uniformly with values ranging from 290 K for the minimum to 295 K for the maximum for both days too.

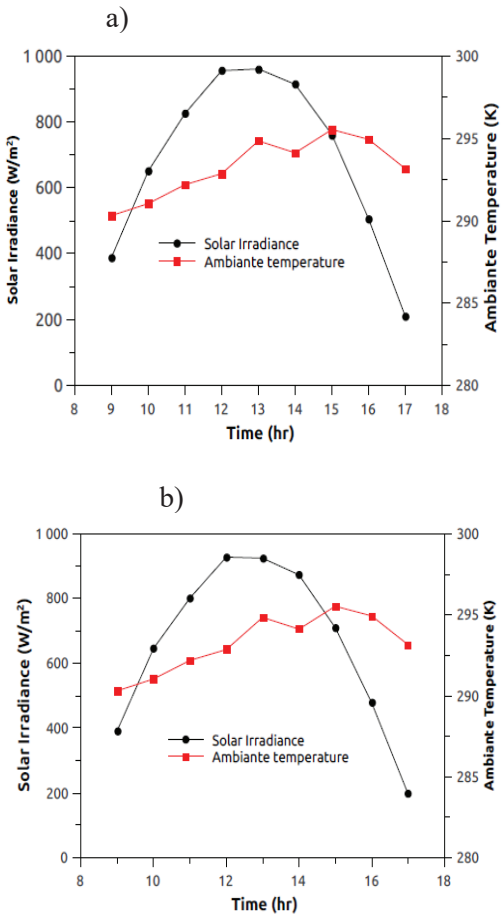

Fig. 2 : Solar irradiance, and ambient temperature; **a)** on 30/12/2021, **b)** on 04/01/2022.

5. Numerical Validation

The validation of the code requires its implementation on an existing experimental model under operating conditions, namely solar radiation and ambient temperature. We conducted a numerical study using data from the Manzanares prototype for September 2, 1982, as used in the reference work for validation [7]. The transient numerical results for the fluid movement established in the Manzanares prototype are presented, including the required validation with appropriate experimental results. The numerical results for the air temperature at the chimney inlet section, spanning from 9 AM to 6 PM, follow the same trend as the experimental results of Haaf [7], with an average deviation of 2% (Fig. 3). The results obtained for the air velocity in the same section are presented in Fig. 4. The maximum average deviation is 17%. Figure 5 displays the expected power from the current simulation and that given by Haaf [7]. We observe the same trend and an average deviation of about 13%.

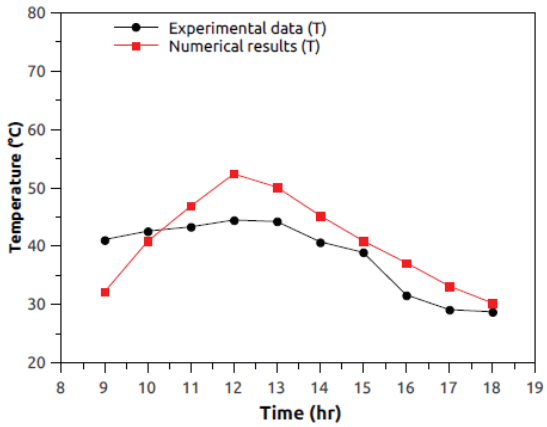

Fig. 3 : Present study temperature and experimental chimney temperature[7] over time.

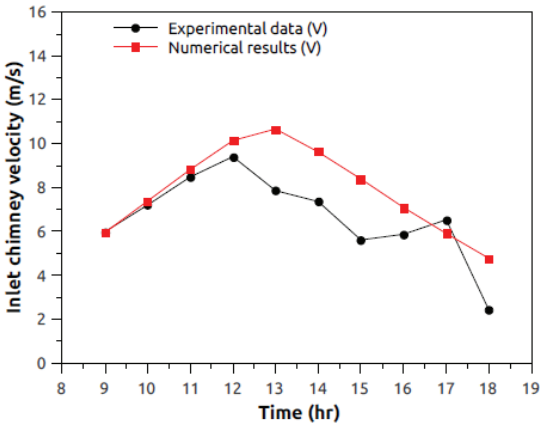

Fig. 4 : Present study velocity and experimental chimney velocity[7] over time.

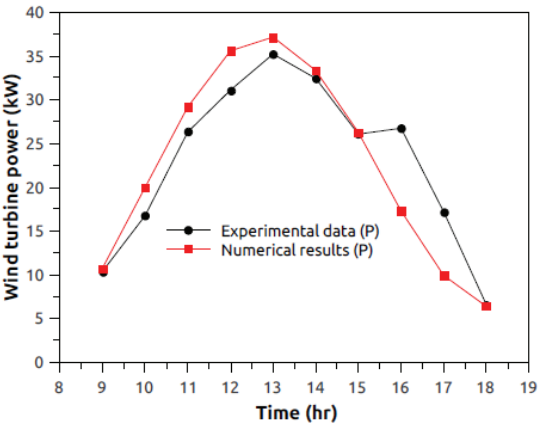

Fig. 5 : Present study power and experimental chimney power[7] over time.

We can conclude that the numerical model developed in this study can be considered valid due to the successful comparison with experimental data obtained in the Manzanares pilot plant.

6. Results and Discussion

A simulation of a solar chimney power plant was undertaken using the fluent computational code. The simulation period covers two days (30-12-2021 and 04-01-2022) from 9 a.m. to 5 p.m. Therefore, the boundary conditions are dependent on meteorological data. The air entering the collector is assumed ambient temperature, with zero relative pressure at the collector inlet and at the chimney outlet. The ground temperature at a depth of 5 meters is assumed constant at 300K. The chimney walls are considered adiabatic. As mentioned previously, the collector is characterized by a transparent cover and an absorbent soil through the product of the soil absorptivity and the cover transmissivity $\tau\alpha$=0.64.

Two scenarios are considered in the simulation. The first one is a solar chimney power plant without any crop growth and the second one with tomato cultivation on the collector soil.

Figure 6 shows the variation of the fluid temperature at the collector outlet for the two considered days, namely 30-12-2021 (Fig.6a) and 04-01-2022 (Fig.6b), respectively. The temperature changes following the same path as the solar radiation does for both configurations. The maximum temperatures are around 320 K for the December day and 318 K for the January day, coinciding with the peak solar radiation recorded around 1 p.m. However, beyond this time, solar radiation decreases as sunset approaches, affecting the fluid temperatures inside the collector in a similar trend. Nevertheless, in the power plant with vegetation, the fluid temperatures decrease with the decrease in solar radiation, but this decrease is not as abrupt as observed in the SCPP without crop cultivation. The temperature difference observed when the radiation starts declining, between the two power plant configurations models averages around 8 K because vegetation cover acts partly as thermal storage. It receives the incident solar radiation that passes through the transparent cover, as well as the energy stored in the ground ~~soil~~ transmitted by plant transpiration. The latter, corresponds to the energy (amount of water) absorbed by the plant from the soil and transferred by the leaves to the atmosphere. Plant transpiration, regulating its temperature, plays a crucial role in water movement and mineral transport in plants. It closely depends on air temperature and humidity [63].

Hence, the stored heat will be transferred to the heat transfer fluid when the energy source begins to weaken or to decrease, as the fluid in motion passes through the vegetation while going through the collector.

Consequently, the temperature drop observed in the collector in the presence of vegetation during periods of intense sunlight results from the absorption, not only by the soil but also by the vegetation, of a certain quantity of the solar radiation flux. This absorbed energy is used as latent heat of vaporization for the plant evapotranspiration. The remaining absorbed radiation transforms into sensible heat through convection to the air. On the contrary for the case without vegetation, in which only the soil absorbs the transmitted solar flux.

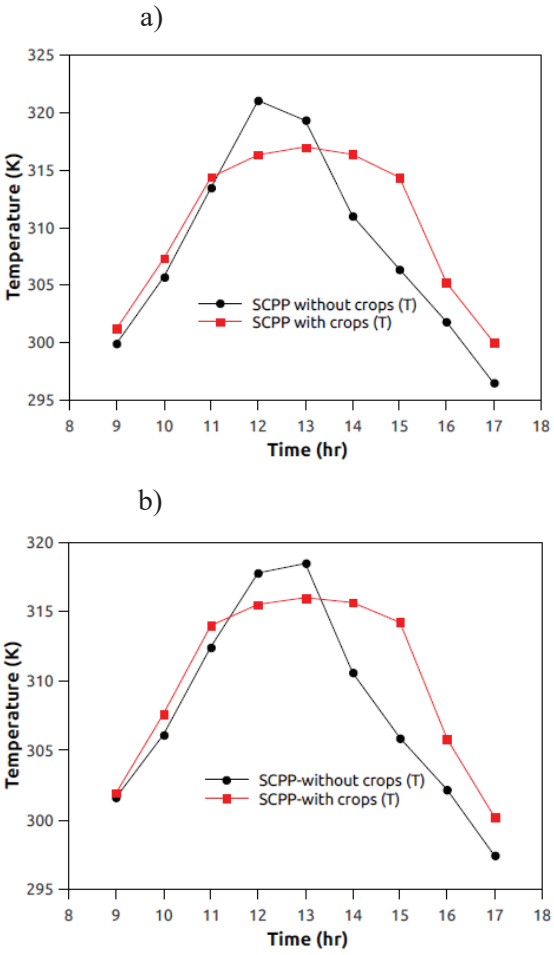

Fig. 6 : Collector outlet temperatures in both configurations; a) on 30/12/2021, b) on 04/01/2022.

Figure 7 shows the instantaneous efficiency variation of the collector for both types of power plants (with and without vegetation) during the two considered days. It is noticeable that the efficiency is significantly higher for the power plant without vegetation, especially during periods of intense sunlight. This is due to the absence of vegetation, which would act as a flow attenuator and obstructs fluid flow, directly affecting directly the flow rate. On the other hand, radiation received in the collector

by the greenhouse effect increases the fluid temperature, that is to say the air. As it heats up, its density decreases, allowing it to move towards the collector's exit. However, in the power plant with vegetation, part of the collected energy will be transferred to the fluid, while the vegetation itself, through the phenomenon of plant transpiration as previously explained, will absorb another part.

Thus, the energy transferred to the fluid will be less significant than in the case without vegetation. Therefore, the combination of these two phenomena, namely the reduction in fluid flow velocity due to vegetation partially obstructing the flow and its absorption of part of the received energy, will impact directly the collector efficiency, given that the latter is proportional to the mentioned parameters, especially the speed and the incident heat flux (eq. 29).

$$\eta_c = \frac{\dot{m}\, C_p (T_o - T_a)}{A_c I_G} \tag{29}$$

where η_c is the collector efficiency, T_o is the temperature collector outlet, T_a is the ambient temperature, A_c is the collector area, I_G is the solar irradiance, C_p is the specific heat capacity of the air and $\dot{m}$ is the mass flow rate.

On the other hand, beyond a certain time, precisely after 2 pm, higher efficiency is observed in the power plant with crop cultivation. In the case of the power plant without vegetation, after 2 pm, the radiation intensity starts gradually decreasing, and consequently, the fluid temperature steadily drops, since it is related to the solar radiation intensity (the only heat source), resulting in a lesser variation in fluid density. Thus, a decrease in the variation of the fluid density will result in lower flow velocities. However, in the case of the power plant with vegetation, despite the reduction in heat generated by incident solar radiation after 2 pm, the air velocities remain constant as it continues to benefit from the heat transmitted by the vegetation (evapotranspiration).

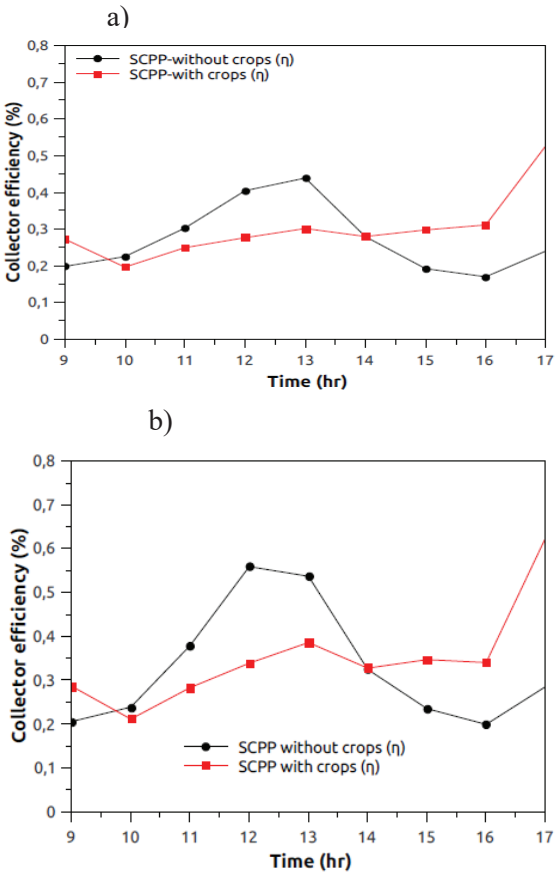

Fig. 7 : Collector efficiency in both configurations; a) on 30/12/2021, b) on 04/01/2022.

As expected, energy production increases with rising solar radiation in all configurations. However, the maximum power is achieved in the system without vegetation during the period of intense sunlight (Fig. 8). Nevertheless, once the solar source begins to decrease, after 2 pm, the system with vegetation takes the lead, with significant energy production. This goes hand in hand with the explanation previously provided concerning the aforementioned parameters, particularly temperatures, velocities, and collector efficiency. It is noteworthy that the generated electrical power is proportional to these parameters as defined by Equation 30 [9].

$$P_{ele} = \frac{2}{3} . \frac{\eta\, g\, H_{ch}}{C_p T_a} A_c I_G \tag{30}$$

where η is the chimney efficiency, g is the gravitational acceleration. The generated power scales with the collector area A_c and the chimney height H_{ch}.

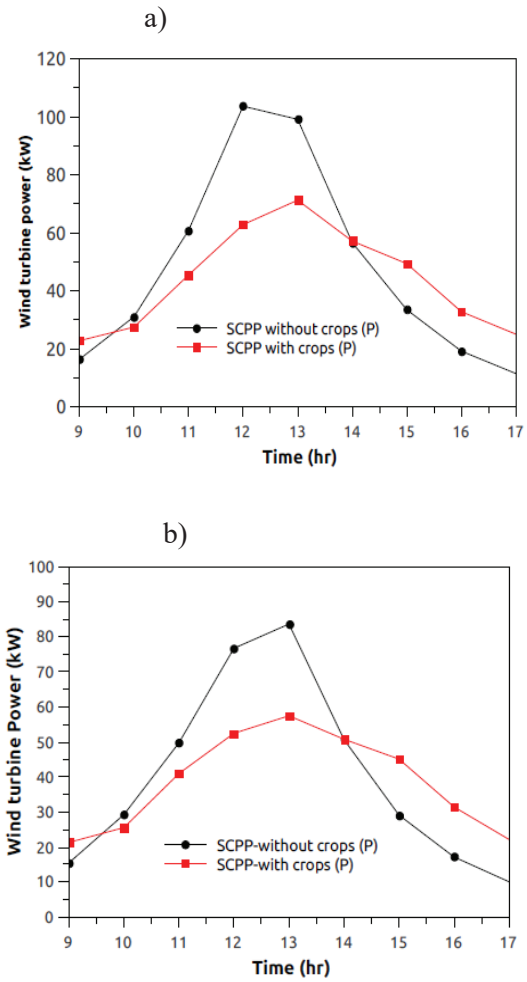

Fig. 8 : Power production in both configurations; a) on 30/12/2021, b) on 04/01/2022.

Analysis of the results shows that the main parameters of the heat transfer fluid (temperature and velocity) evolve proportionally to solar radiation during the period from 9 AM to 5 PM for all configurations. This will directly affect the collector's efficiency and consequently the electrical energy generated by the generators.

However, during the period of intense sunlight, the system without vegetation yields the best results in terms of heat transfer fluid temperatures at the collector outlet, a better flow rate, as well as better thermal efficiency of the collector, and consequently, better electrical energy production. Nevertheless, once solar radiation begins to decrease in intensity (beyond 2 PM), the best results (temperature, velocity, collector efficiency, and electrical power) are obtained with the system with crop vegetation.

Based on the considered period, the results are globally nearly the same, whether for the system without vegetation or the system with vegetation. Therefore, it can be observed that the system with vegetation is more advantageous compared to the one without vegetation. Incorporating crop cultivation at the collector level will increase the overall efficiency of the solar chimney power plant and lower the cost per kilowatt-hour produced, consequently reducing the payback period of the initial investment, which is relatively high for this type of installation.

Figures (9-11) show the evolution of the relative static pressure, temperature, and velocity inside the collector in the system with crop cultivation. The measurements are obtained when solar radiation reaches its peak (1 PM), with the aim of estimating the effect of these parameters on the tomato plant.

Figure 9 shows the variation of static pressure in the collector for the two days considered, Fig. 9a, for the day in December and Fig. 9b for the day in January. The air enters at atmospheric pressure, and its pressure decreases as it moves towards the collector's exit. The minimum static pressure is reached at the chimney's entrance (collector's exit).

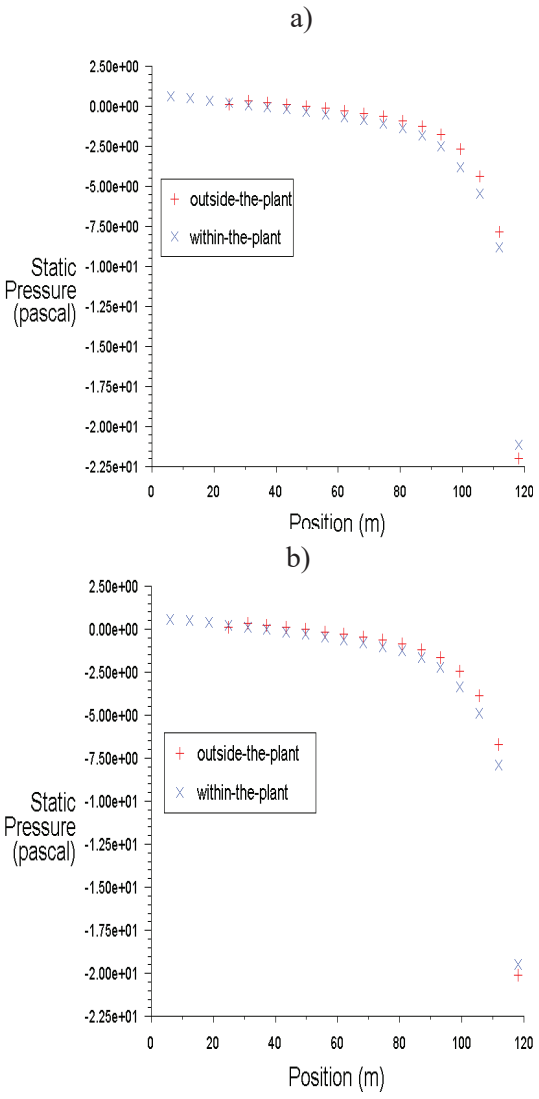

Fig. 9 : Relative static pressure in the configuration with vegetation; a) on 30/12/2021, b) on 04/01/2022.

Figure 10 represents the temperature evolution within the vegetation and in the area between the two sets of vegetation. We observe that the temperatures within the vegetation are higher than those recorded in the empty space. The maximum temperatures obtained are around 314 K. This indicates that the heat transfer fluid absorbs heat from the plant through the mentioned transfer modes. This is confirmed by its temperature drop beyond its passage through the vegetation. On the other hand, in the empty space, the fluid temperature gradually increases up to the collector exit.

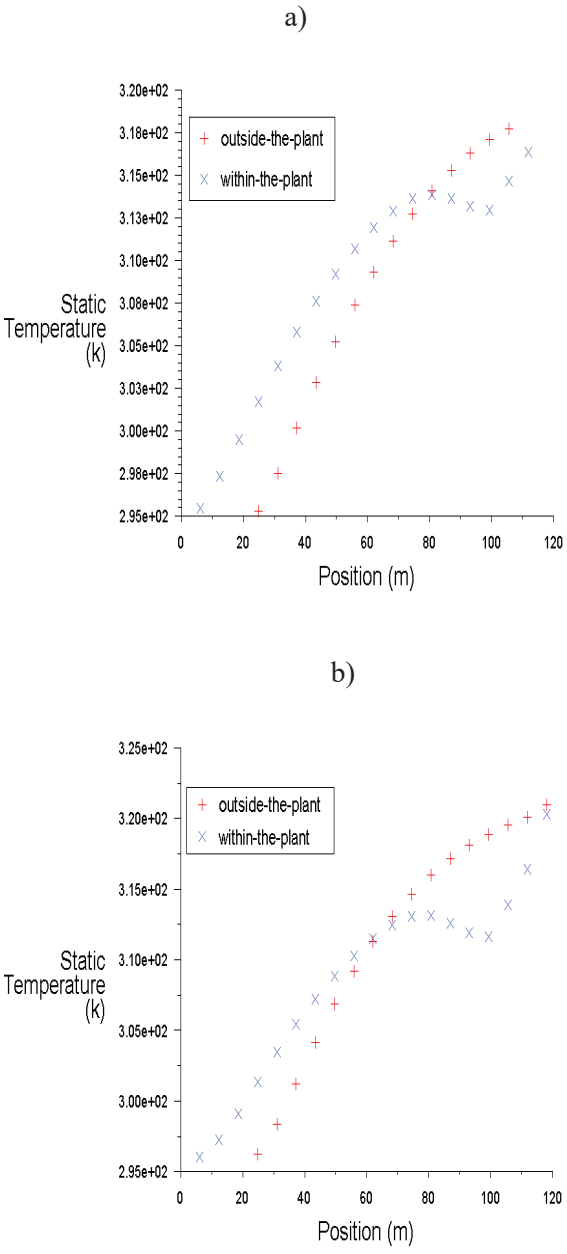

Fig. 10 : Static temperature in the configuration with vegetation; a) on of 30/12/2021, b) on 04/01/2022.

Figure 11 shows the evolution of the velocity at the two locations considered. Flow velocities are significantly higher in the space between the sets of vegetation; however, within the vegetation, very low velocities are recorded, barely exceeding 1 m/s.

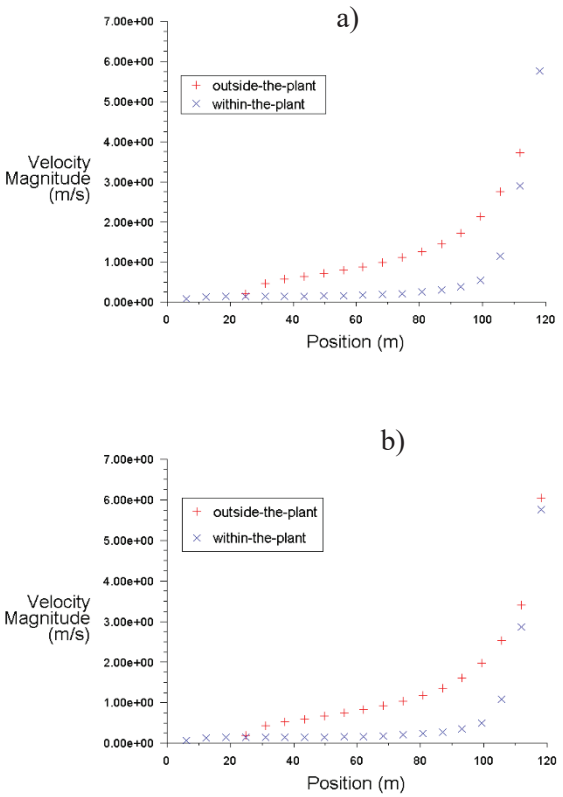

Fig. 11 : Velocity in the configuration with vegetation; a) on 30/12/2021, b) on 04/01/2022.

Based on the analysis of these results, it can be concluded that the environment within the collector is favorable for the plant's growth.

7. Conclusion

The numerical simulation conducted in the context of this study on the solar chimney power plant with and without crop cultivation provided interesting results, highlighting the significance of innovation and integration of renewable energy with agriculture. The variations in temperature and fluid velocity inside the collector were closely linked to changes in solar radiation, displaying the dynamic nature of solar energy utilization. The presence of vegetation, represented here by a tomato crop, notably influenced fluid velocity, with lower speeds observed within the vegetation, suggesting potential impacts on system performance.

Moreover, the study revealed that integrating vegetation within the solar chimney power plant could lead to thermal and energy advantages. While the collector's efficiency exhibited differences based

on solar radiation levels throughout the day, the presence of vegetation demonstrated superior performance during periods of reduced sunlight, highlighting the potential benefits of this hybrid approach.

Thus, incorporating crop cultivation vegetation at the collector level can lower the kilowatt-hour (kWh) cost and reduce the payback period of the initial investment. This aspect is crucial for addressing the drawback of high implementation costs associated with renewable energy technologies. From an environmental perspective, the integration of solar chimney power plants with agriculture contributes to better land use efficiency, promoting sustainable practices and biodiversity conservation. By leveraging innovation in renewable energy systems and agricultural techniques, we can optimize resource utilization and reduce environmental impacts associated with conventional energy production methods. This study underscores the importance of innovation and interdisciplinary collaboration in advancing renewable energy solutions. By integrating solar chimney power plants with agriculture, we not only enhance energy production efficiency but also promote economic viability, environmental sustainability, and food security. This hybrid approach represents a promising avenue for further exploration and underscores the potential for transformative change in the field of solar energy.

Nomenclature

A	area (m^2)
b	thermal penetration coefficient $\left(Ws^{\frac{1}{2}}K^{-1}m^{-2}\right)$
b	thermal penetration coefficient $\left(Ws^{\frac{1}{2}}K^{-1}m^{-2}\right)$
C	density of sensible heat flux $(w.m^{-2})$
c_p	specific heat $(\mathrm{j.kg^{-1}k^{-1}})$
D_w	diffusion coefficient $(m^2 . s^{-1})$
D_h	hydraulic diameter (m)
E	the evaporation flux $(kg.m^{-2}.s^{-1})$
f	volume forces$(\mathrm{kg.m^{-2}.s^{-2}})$
g	gravitational acceleration $(\mathrm{m.s^{-2}})$
$G(z)$	radiation at the height z of the plant $(w.m^{-2})$
H_{ch}	height of chimney (m)
h	heat transfer coefficient $(w.m^{-2}.K^{-1})$
j	mass flux $(kg\ m^{-2}\ s^{-1})$
K	turbulent kinetic energy $(\mathrm{j.kg^{-1}}.m.s^{-2})$
K_c	radiation extinction coefficient
L	length scale(m)
LAI_s	leaf area index
LAI_v	volumetric leaf area index
L_V	heat of vaporization of water $(KJ.kg^{-1})$
M	Mach number
P	pressure (pa)
P_r	Prandtl number
R	Solaire irradiance $(w.m^{-2})$
r	resistance to transfer $(S.m^{-2}kg^{-1})$
Ra	Rayleigh number
r_a	aerodynamic resistance $(s.m^{-1})$
R_n	net radiation $(w.m^{-2})$
Re	Reynolds number
$S_{w,p}$	source term (W)
T	temperature (k)
u, v and w	velocity components $(\mathrm{m.s^{-1}})$
U	heat transfer coefficient $(\mathrm{w.m^{-2}.k^{-1}})$
W	absolute humidity $\left(kg_{water}.kg_{dry-air}^{-1}\right)$

Greek symbols

λ	thermal conductivity $(\mathrm{W.M^{-1}.K^{-1}})$
ΔT	temperature difference (K)
Δp	pressure difference in the chimney (Pa)
ρ	volumetric density $(kg.m^{-3})$
α	thermal diffusivity $(\mathrm{M^2.S^{-1}})$
v	kinematic viscosity $(\mathrm{M^{-2}.S^{-1}})$
ε	turbulent dissipation rate $(\mathrm{M^2.S^{-3}})$
μ	dynamic viscosity $(\mathrm{Kg.M^{-1}.S^{-1}})$
β	thermal expansion coefficient $(\mathrm{K^{-1}})$
Ø	energy dissipation (W)
Φ	porosity
	efficiency

Subscripts

a	air
b	ground
c	cold
ch	chimney
$coll$	collector
$elec$	electric
f	leaf
max	maximum
min	minimum
t	total
∞	environment

References

1) K. Hideo, S.T., T. Kazuki, J. Woojong, N. Hirofumi, M. Shintaro, and M. Kana Moroga, "Possibility of Cooperation for a Low Carbon Society Comparison of the Fukuoka and Busan Metropolitan Cities. *Journal of Novel Carbon Resource Sciences*", 2(21-35).(2010).DOI:
2) A.S. Abdelgader, et al., "Impact of Internal Combustion Engine on Energy Supplyand its

Emission Reduction via Sustainable Fuel Source. *Evergreen*", 9(3): p. 830-844.(2022).DOI: 10.5109/4843114

3) Shalom, A., "Navigating the Potential Applications and Challenges of Intelligent and Sustainable Manufacturing for a Greener Future. *EVERGREEN Joint Journal of Novel Carbon Resource Sciences & Green Asia Strategy*", 10(4): p. 2237-2243.(2023).DOI:
4) A. Jhalanim, et al., "Energy Security Scenarios for India Under Diversified Demand and Supply. *Evergreen*", 10(4): p. 2683-2689.(2023).DOI: 10.5109/7160927
5) Y. Wibisono, et al., "Activated Carbon Loaded Mixed Matrix Membranes Extracted from Oil Palm Empty Fruit Bunches for Vehicle Exhaust Gas Adsorbers. *Evergreen*", 8(3): p. 593-600.(2021).DOI: 10.5109/4491651
6) K. Marzia, M.F.H., T. Miyazaki, B.B. Saha, and S. Koyama, "Key Factors of Solar Energy Progress in Bangladesh until 2017. *Evergreen*", 5(2): p. 78-85.(2018).DOI: 10.5109/1936220
7) Haaf, W., "Solar chimneys-part II : preliminary test result from Manzanares pilot plant. . *International Journal of Solar Energy*", 2(2): p. 141-161.(1984).DOI: 10.1080/01425918408909921
8) W. Haaf, K.F., G. Mayr, and J. Schlaich, "Solar Chimneys Part I: Principle and Construction of the Pilot Plant in Manzanares. *International Journal of Solar Energy*", 2(1): p. 3-20.(2007).DOI: 10.1080/01425918308909911
9) M. K. Hasan, A.G., L. Bahrainirad, and H. F. Fasel, ""Investigation of collector flow for 1:30 scale solar chimney power plant model". *Solar Energy*", 241: p. 220-230.(2022).DOI: 10.1016/j.solener.2022.05.059
10) E. Abdelsalam, F.A., and S. Ibrahim, "A novel hybrid solar chimney power plant: Performance analysis and deployment feasibility. *Energy Science & Engineering*", 10(9): p. 3559-3579.(2022).DOI: 10.1002/ese3.1240
11) S. Mehranfar, A.G., A. Azizi, A.Mahmoudzadeh Andwari, A. Pesyridis, and H. Jouhara, "Comparative assessment of innovative methods to improve solar chimney power plant efficiency. *Sustainable Energy Technologies and Assessments*", 49: p. 101807.(2022).DOI:10.1016/j.seta.2021.101807
12) A.A.M. Omara, H.A.M., I.J. Al Rikabi, M.A. Abuelnour, and A.A.A. Abuelnuor, "Performance improvement of solar chimneys using phase change materials: A review. *Solar Energy*", 228: p. 68-88.(2021).DOI: 10.1016/j.solener.2021.09.037
13) A. A. Ismaeel, H.A.A.W., and Z. H. Naji, "Performance Evaluation of Updraft Air Tower Power Plant Integrated with Double Skin Solar Air Heater. *Evergreen*", 8(2): p. 296-303.(2021).DOI: 10.5109/4480706
14) A. J. Hussein, A.I.A., L.S. Ahlam "Review of Hybrid Photovoltaic- Air Updraft Solar Application: Present and Proposed state Models. *EVERGREEN Joint Journal of Novel Carbon Resource Sciences & Green Asia Strategy*", 9 (4): p. 1181-1202.(2022).DOI: doi.org/10.5109/6625729
15) F. Murena, I.G., and B. Mele, "Fluid dynamic performances of a solar chimney plant: Analysis of experimental data and CFD modelling. *Energy*", 249: p. 123702.(2022).DOI: 10.1016/j.energy.2022.123702
16) A. Ridwan, H.H., and M.R. Fauzi, "Design and experimental test for solar chimney power plant: case study in Riau Province, Indonesia. *IOP Conference Series: Materials Science and Engineering*", 403: p. 012092.(2018).DOI: 10.1088/1757-899x/403/1/012092
17) M. Sundararaj, N.R., J. Anbarasi, S. Yaknesh, and R. Sathyamurthy, "Parametric optimization of novel solar chimney power plant using response surface methodology. *Results in Engineering*", 16: p. 100633.(2022).DOI: 10.1016/j.rineng.2022.100633
18) K. Kazemi, M.E., M. Lahonian, and A. Babamiri, "Micro-scale heat and electricity generation by a hybrid solar collector-chimney, thermoelectric, and wind turbine. *Sustainable Energy Technologies and Assessments*", 53: p. 102394.(2022).DOI:10.1016/j.seta.2022.102394
19) D. Pritam, a.V.P.C., "3D numerical study on estimating flow and performance parameters of solar updraft tower (SUT) plant: Impact of divergent angle of chimney, ambient temperature, solar flux and turbine efficiency. *Journal of Cleaner Production*", 256: p. 120353.(2020).DOI:10.1016/j.jclepro.2020.120353
20) L.K. Hooi, a.S.K.T., "A parametric simulation of solar chimney power plant. *IOP Conference Series: Materials Science and Engineering*", 297: p. 012057.(2018).DOI: 10.1088/1757-899x/297/1/012057
21) M. Tingzhen, R.K.d.R., F. Meng, Y. Pan, and W. Liu, "Chimney shape numerical study for solar chimney power generating systems. *International Journal of Energy Research*", 37(4): p. 310-322.(2013).DOI: 10.1002/er.1910
22) R. Natarajan, a. V. Jayaraman, and R. Sathyamurthy, "Comparative studies on

performance of solar towers with variable scale ratios. *Environ Sci Pollut Res Int*", 29(30): p. 45601-45611.(2022).DOI: 10.1007/s11356-022-19079-0

23) H. Semai and A. Bouhdjar, "Impact of the chimney geometry on the power output of solar chimney power plant. *Thermophysics and Aeromechanics*", 28(2): p. 291-303.(2021).DOI: 10.1134/s0869864321020128
24) K. Sajjan Raj, V.P.C., and D. Pritam, "A 3D numerical study to evaluate optimum collector inclination angle of Manzanares solar updraft tower power plant. *Solar Energy*", 226: p. 455-467.(2021).DOI: 10.1016/j.solener.2021.08.062
25) D. Pritam, a.V.P.C., "Estimation of flow parameters and power potential of solar vortex engine (SVE) by varying its geometrical configurations: A numerical study. *Energy Conversion and Management*", 223: p. 113272.(2020).DOI:10.1016/j.enconman.2020.113272
26) R. Balijepalli, V.P.C., K. Kirankumar, and S. Suresh, "Numerical analysis on flow and performance characteristics of a small-scale solar updraft tower (SUT) with horizontal absorber plate and collector glass. *Journal of Thermal Analysis and Calorimetry*", 141(6): p. 2463-2474.(2020).DOI: 10.1007/s10973-020-10057-7
27) A. Ayadi, Z.D., A. Bouabidi, and M.S. Abid, "Effect of the number of turbine blades on the air flow within a solar chimney power plant. *Proceedings of the Institution of Mechanical Engineers, Part A: Journal of Power and Energy*", 232(4): p. 425-436.(2017).DOI: 10.1177/0957650917733128
28) Raed, A.J., "Experimental Study of Wind Turbine Power Generation Utilizing Discharged Air of Air Conditioner Blower. *EVERGREEN Joint Journal of Novel Carbon Resource Sciences & Green Asia Strategy*", 9(4): p. 1103-1109.(2022).DOI: doi.org/10.5109/6625722
29) A. Ganguli, S.D., and A. Pandit, "CFD Simulations for Performance Enhancement of a Solar Chimney Power Plant (SCPP) and Techno-Economic Feasibility for a 5 MW SCPP in an Indian Context. *Energies*", 14(11): p. 3342.(2021).DOI: 10.3390/en14113342
30) P. Guo, Y.W., J. Li, and Y. Wang, "Thermodynamic analysis of a solar chimney power plant system with soil heat storage. *Applied Thermal Engineering*", 100: p. 1076-1084.(2016).DOI:10.1016/j.applthermaleng.2016.03.008
31) C.O. Okoye, O.S., and O. Taylan, "A new economic feasibility approach for solar chimney power plant design. *Energy Conversion and Management*", 126: p. 1013-1027.(2016).DOI: 10.1016/j.enconman.2016.08.080
32) H. Semai and A. Bouhdjar, "Effect of slope tower angle and thermal storage media on flexibility solar chimney power plant performance. *Environmental Progress & Sustainable Energy*", 40(5).(2021).DOI: 10.1002/ep.13646
33) M.J. Maghrebi, a.R.M.N., "Performance evaluation of floating solar chimney power plant in Iran: estimation of technology progression and cost investigation. *IET Renewable Power Generation*", 11(13): p. 1659-1666.(2017).DOI: 10.1049/iet-rpg.2016.0963
34) V. Putkaradze, P.V., A. Mammoli, and N. Fathi, "Inflatable free-standing flexible solar towers. *Solar Energy*", 98: p. 85-98.(2013).DOI: 10.1016/j.solener.2013.07.010
35) Bouchair, A., "The effect of the altitude on the performance of a solar chimney. *Energy*", 249: p.123704.(2022).DOI:10.1016/j.energy.2022.123704
36) X. Zhou, a.J.Y., "A Novel Solar Thermal Power Plant with Floating Chimney Stiffened onto a Mountainside and Potential of the Power Generation in China's Deserts. *Heat Transfer Engineering*", 30(5): p. 400-407.(2009).DOI: 10.1080/01457630802414813
37) C.G. Granqvist, a.G.A.N., "Solar energy materials for thermal applications: A primer. *Solar Energy Materials and Solar Cells*", 180: p.213-226.(2018). DOI:10.1016/j.solmat.2018.02.004
38) K. Ikhlef, S.L., and I. Üçgül, "Experimental study of different thermal storage system effects on the performance of a small prototype solar chimney power plant. *Renewable Energy*", 200: p.516-526.(2022).DOI: 10.1016/j.renene.2022.09.087
39) A. Azani, et al., "The Effect of GO/TiO_2 Thin Film During Photodegradation of Methylene Blue Dye. *Evergreen*", 8(3): p. 556-564.(2021).DOI: 10.5109/4491643
40) B.M. Flohr, E.A.M., J.R. Hunt, T.M. McBeath, and R.S. Llewellyn, "A modelled quantification of reduced nitrogen fertiliser requirement and associated trade-offs from inclusion of legumes and fallows in wheat-based crop sequences *Field Crops Research*", 307 (2024).DOI: 10.1016/j.fcr.2023.109236
41) Y., Y., R. Youngryel, L. Bolun, D. Benjamin, Z. Sheir Afgen, and K. Minseok, "A multi-objective optimization approach to simultaneously halve water consumption, CH4, and N2O emissions while maintaining rice yield. *Agricultural and Forest Meteorology*", 344: p.

109785.(2024).DOI:10.1016/j.agrformet.2023.109785
42) L. Zhang, Y.M., Z. Chen, X. Hu, C. Wang, and L. C. Wang, "A systematic review of life-cycle GHG emissions from intensive pig farming: Accounting and mitigation. *Sci Total Environ*", 907: p. 168112.(2024).DOI: 10.1016/j.scitotenv.2023.168112
43) O.A. Ogbolumani, a.N.L.N., "Environmental impact assessment for a meta-model-based food-energy-water-nexus system. *Energy Reports*", 11: p. 218-232.(2024).DOI: 10.1016/j.egyr.2023.11.033
44) F. Ziegler, A.A.N., M. Langeland, Y. Wocken, E.S. Hognes, and S. Mehta, "Greenhouse gas emission reduction opportunities for the Norwegian salmon farming sector - can they outweigh growth? *Aquaculture*", 581: p. 740431.(2024).DOI: 10.1016/j.aquaculture.2023.740431
45) S. Locatelli, W.B., L. Verdi, C. Nicoletto, A. Dalla Marta, and C. Maucieri, , "Modelling the response of tomato on deficit irrigation under greenhouse conditions. *Scientia Horticulturae*", 326:p.112770.(2024).DOI:10.1016/j.scienta.2023.112770
46) W.J. Yuan, Z.Y.H., S.P. Zhang, Y.P. Zheng, X.Q. Zhang, S.Q. He, Y.X. He, and Y. Li, "Comparative transcriptomics provides insights into the pathogenic immune response of brown leaf spots in weeping forsythia. *Tree Physiol*", 43(9): p. 1641-1652.(2023).DOI: 10.1093/treephys/tpad060
47) A. Berisha, a.L.O., "Kosovo Scenario for Mitigation of Greenhouse Gas Emissions from Municipal Waste Management. *Evergreen*", 8(3): p. 509-516.(2021).DOI: 10.5109/4491636
48) Anderson, R.L., "Synergism: A Rotation Effect of Improved Growth Efficiency. *Advances in Agronomy*", 112: p. 205-226.(2011).DOI: 10.1016/b978-0-12-385538-1.00005-6
49) S. L. Gilhespy, S.A., L. Cardenas, D. Chadwick, A. del Prado, C. Li, T. Misselbrook, R. M. Rees, W. Salas, A. Sanz-Cobena, P. Smith, E. L. Tilston, C. F.E. Topp, S. Vetter, and J.B. Yeluripati, "First 20 years of DNDC (DeNitrification DeComposition)_ Model evolution. *Ecological Modelling*", 292 p. 51–62.(2014).DOI: http://dx.doi.org/10.1016/j.ecolmodel.2014.09.004
50) T. B.T. Vo, K.J., R. Wassmann, B.O. Sander, and F. Asch, "Varietal effects on Greenhouse Gas emissions from rice production systems under different water management in the Vietnamese Mekong Delta. *Journal of Agronomy and Crop Science*", 210(1).(2023).DOI: 10.1111/jac.12669
51) X. Díaz de Otálora, A.d.P., F.vDragoni, L. Balaine, G. Pardo, W. Winiwarter, A. Sandrucci, G. Ragaglini, T. Kabelitz, M. Kieronczyk, G. Jørgensen, F. Estellés, and B. Amon, "Modelling the effect of context-specific greenhouse gas and nitrogen emission mitigation options in key European dairy farming systems. *Agronomy for Sustainable Development*", 44(1).(2024).DOI: 10.1007/s13593-023-00940-6
52) A. Mukhtiar, A.M., M.A. Zia, M. Ameen, R. Dong, Y. Shoujun, M.M. Javaid, B.A Khan, and M.A. Nadeem, "Role of biogas slurry to reclaim soil properties providing an eco-friendly approach for crop productivity. *Bioresource Technology Reports*", 25: p. 101716.(2024).DOI:10.1016/j.biteb.2023.101716
53) B. Nervo, A.L., A. Roggero, C. Palestrini, and A. Rolando, "Spatio-temporal modelling suggests that some dung beetle species (Coleoptera: Geotrupidae) may respond to global warming by boosting dung removal. *Sci Total Environ*", 908: p. 168127.(2024).DOI: 10.1016/j.scitotenv.2023.168127
54) G. Casazza, E.Z., M.G. Mariotti, F. Médail, and L. Minuto, Luigi, "Ecological and historical factors affecting distribution pattern and richness of endemic plant species: the case of the Maritime and Ligurian Alps hotspot. *Diversity and Distributions*", 14(1): p. 47-58.(2007).DOI:10.1111/j.1472-4642.2007.00412.x
55) T. Carlos, R.E.A., S.L. Lucía, and U. Antonio, "Photovoltaic technology as a tool for ecosystem recovery: A case study for the Mar Menor coastal lagoon. *Applied Energy*", 356: p. 122350.(2024).DOI:10.1016/j.apenergy.2023.122350
56) Hermann, S., "Boundary layer theory *McGraw-Hill Science-Engineering-Math*".(1979).DOI:
57) S.H. Danook, H.A.Z.A.-b., I. Hashim, and D. Veeman, "CFD Simulation of a 3D Solar Chimney Integrated with an Axial Turbine for Power Generation. *Energies*", 14(18): p. 5771.(2021).DOI: 10.3390/en14185771
58) Saugier, B., *Transports turbulents de CO2 et de vapeur d'eau au-dessus et à l'intérieur de la végétation. Méthodes de mesure micrométéorologiques*, Gauthier-Villars, Editor 1970.
59) T. Boulard, A.B., M. Mermier, and F. Villette, "Mesures et modélisation de la résistance stomatique foliaire et de la transpiration d'un

couvert de tomates de serre. *Agronomie*", 11(4): p.259-274.(1991).DOI: 10.1051/agro:19910403
60) H. Meidner, a.T.A.M., "Physiology of Stomata. *McGraw-Hill, London.*".(1968).DOI:
61) H. Lange, W.S., JR. and H. Mohr, "An Analysis of Phytochrome-mediated Anthocyanin Synthesis. *Plant Physiol.* ", 47: p. 649-655.(1971).DOI:
62) Turner, N.C., "Measurement and influence of environmental and plant factors on stomatal conductance in the field. *Agricultural and Forest Meteorology* ", 54 p. 137-154.(1991).DOI:
63) M.A. Lamrani, T.B., J.C. Roy, and A. Jaffrin, "Air Flows and Temperature Patterns induced in a Confined Greenhouse. *Journal of Agricultural Engineering Research*", 78(1): p. 75-88.(2001).DOI: 10.1006/jaer.2000.0568